Supporting Information for "Cooling crusts create concomitant cryovolcanic conduits"

Maxwell L. Rudolph[1], Michael Manga[2], Matthew Walker[3], and Alyssa R. Rhoden[4]

[1]Department of Earth and Planetary Sciences, University of California, Davis CA

[2]Department of Earth and Planetary Science, University of California, Berkeley CA

[3]Planetary Science Institute, Tucson AZ

[4]Southwest Research Institute, Boulder CO

Contents of this file

Introduction

In Text S1, we provide an analytic solution for the steady-state diffusion equation in an ice shell with temperature-dependent thermal conductivity. In Text S2, we derive the momentum conservation equation. The verification/benchmarking of our numerical code is described in Text S3. In Text S4, we consider thickening ice shells with no tidal dissipation.

Text S1: Steady conduction with temperature-dependent thermal conductivity

For thermal conductivity with the functional form $k(T) = k_1/T$, a steady-state solution can be found to satisfy

$$\frac{d}{dr}\left(r^2 \frac{k_1}{T}\frac{dT}{dr}\right) = 0, \tag{S1}$$

subject to temperature boundary conditions $T(R_i) = T_b$ at the inner radius R_i and $T(R_o) = T_S$ at the outer radius R_o. The solution has the functional form

$$\ln(T) = \frac{c_0}{r} + c_1 \tag{S2}$$

where the constants c_0 and c_1 are given by

$$c_0 = \frac{R_i R_o}{R_i - R_o}(\log T_S - \log T_b) \tag{S3}$$

$$c_1 = \ln T_s - \frac{c_0}{R_o}. \tag{S4}$$

The heat flux at any radius r may be calculated using $q = \frac{k_1 c_0}{r^2}$.

Text S2: Derivation of the momentum conservation equation

Here we derive the equations governing the thermo-visco-elastic response of a spherical shell. Under the assumption of spherical symmetry, the off-diagonal terms in the stress tensor vanish and the principal stresses act in the radial (σ_r) and azimuthal ($\sigma_\theta, \sigma_\phi$) directions. By symmetry, the stress components acting in the tangential direction are equal ($\sigma_\theta = \sigma_\phi$) and we denote this single tangential stress component as σ_t. Throughout the present work, tensional stresses are positive in sign. Our derivation closely follows Appendix A of Hillier and Squyres (1991) and (Nimmo, 2004) but is repeated here for completeness. Instead of seeking an integro-differential equation, we derive an equation for the radial stress ($\sigma_r(r)$) that is well-suited to numerical discretization using conservative finite differences. The principal strains in the radial and azimuthal directions, ϵ_r and ϵ_t respectively, are given by

$$\epsilon_t = \frac{u_r}{r} \tag{S5}$$

$$\epsilon_r = \frac{du_r}{dr} = \frac{d}{dr}(r\epsilon_t) \tag{S6}$$

The conservation of momentum is expressed through a balance between radial and tangential stresses,

$$\frac{d\sigma_r}{dr} = \frac{2}{r}(\sigma_t - \sigma_r). \tag{S7}$$

Adopting a Maxwell viscoelastic constitutive relation, the radial and tangential stresses are related to strain-rates according to

$$\frac{d\epsilon_t}{dt} = \frac{d}{dt}\left(\frac{1}{E}\left[\sigma_t - \nu(\sigma_t + \sigma_r)\right] + \alpha\right) + \frac{\sigma_t^D}{2\mu} \tag{S8}$$

$$\frac{d\epsilon_r}{dt} = \frac{d}{dt}\left(\frac{1}{E}\left[\sigma_r - 2\nu\sigma_t\right] + \alpha\right) + \frac{\sigma_r^D}{2\mu}. \tag{S9}$$

Here, E is the shear modulus, ν is Poisson's ratio, $\alpha = \alpha_l \Delta T$ for linear coefficient of thermal expansion α, μ is viscosity, and the superscript $(^D)$ denotes the deviatoric stress components. The property α_l is the coefficient of linear thermal expansion (1/3 of the coefficient of volumetric thermal expansion) and $\Delta T = T - T_{ref}$ is the temperature increase relative to a reference temperature T_{ref}. The deviatoric stress components can be obtained using Equation S7 as

$$\sigma_t^D = \frac{r}{6}\frac{d\sigma_r}{dr} \tag{S10}$$

$$\sigma_r^D = -\frac{r}{3}\frac{d\sigma_r}{dr}. \tag{S11}$$

From the definition of the strains, we begin by stating

$$\frac{d}{dt}\epsilon_r = \frac{d}{dt}(\epsilon_t + r\frac{d\epsilon_t}{dr}). \tag{S12}$$

This can be re-arranged to find an expression for the differential strain

$$\frac{d}{dt}(\epsilon_r - \epsilon_t) = r\frac{d}{dt}\frac{d\epsilon_t}{dr}. \tag{S13}$$

We substitute Equations S8-S9 to obtain

$$r\frac{d}{dt}\frac{d\epsilon_t}{dr} = \frac{d}{dt}\left[\frac{1+\nu}{E}(\sigma_r - \sigma_t)\right] + \frac{\sigma_r^D - \sigma_t^D}{2\mu} \tag{S14}$$

which is Equation A10 of Hillier and Squyres (1991). From Equation S7,

$$\sigma_r - \sigma_t = \sigma_r^D - \sigma_t^D = -\frac{r}{2}\frac{d\sigma_r}{dr} \tag{S15}$$

We then substitute Equation S8 for the term involving ϵ_t and eliminate the terms involving σ_t using Equation S7. Denoting time derivative with a dot $(\dot{})$, we write

$$\frac{3(1-\nu)}{2E}\frac{d\dot{\sigma}_r}{dr} + \frac{1-\nu}{E}\frac{d}{dr}\left(\frac{r}{2}\frac{d\dot{\sigma}_r}{dr}\right) + \frac{1}{4\mu}\frac{d\sigma_r}{dr} + \frac{d}{dr}\left(\frac{r}{12\mu}\frac{d\sigma_r}{dr}\right) = -\frac{d\dot{\alpha}}{dr} \tag{S16}$$

We solve Equation S16 using an implicit method. We first introduce a backwards-Euler approximation to all time derivatives and conservative, centered in space finite difference approximations to all spatial derivatives. At each timestep, we solve for σ_r subject to the boundary conditions that $\sigma_r(r_b) = P_{ex}$ where r_b is the time-dependent location of the base of the ice shell and P_{ex} is the ocean overpressure. The radial stress at the surface is zero. Given a solution for σ_r, we can obtain the tangential stress using Equation S7. Then, we use the constitutive relations (Equation S8) to obtain strain-rate and cumulative strain. Finally, we obtain the radial displacement through the definition of strain ($u_r = r\epsilon_t$).

Text S3: Model verification

We verified the correctness of the numerical solution against available analytic solutions and previously published numerical results. The four verification steps described below and documented in the code associated with this manuscript verify the correctness of the temperature solutions and stress solutions independently, the coupling between the temperature and stress equations for a problem without a moving boundary, the correctness of the solution for ice shell thickening, and the consistency of calculations with a cooling viscoelastic shell with published results.

First, we verified that for a purely elastic model (i.e. with $\mu = \infty$), we recover the known analytic solution for stresses and displacements. For a spherical shell with inner radius R_i and outer radius R_0 subject to boundary stresses $\sigma_r(R_i) = -P$ and $\sigma_r(R_o) = 0$, the distribution of stresses is given by

$$\sigma_r(r) = \frac{R_i^3}{R_o^3 - R_i^3}\left(\frac{R_o^3}{r^3} - 1\right) \times (-P). \tag{S17}$$

The tangential stresses and displacements can be obtained from σ_r and its derivatives.

Second, we verified that our code reproduces the solution for thermoelastic stresses in a spherical shell of finite thickness, given in Section 136 of Timoshenko and Goodier (1951). For this benchmark problem, the temperature boundary conditions on the inner and outer surfaces of the spherical shell are given by $T(R_i) = T_i$ and $T(R_o) = 0$. The inner and outer surfaces are subject to zero normal stress ($\sigma_r = 0$). The solution for radial stresses is given by

$$\sigma_r(r) = \frac{\alpha E T_i}{1-\nu}\frac{R_i R_o}{R_o^3 - R_i^3}\left[R_i + R_o - \frac{1}{r}(R_o^2 + R_i R_o + R_i^2) + \frac{R_i^2 R_b^2}{r^3}\right]. \tag{S18}$$

This test verifies the correctness of the coupling between the thermal and mechanical equations in our code.

Third, we verified the results from Nimmo (2004). Nimmo (2004) investigated stresses due to changes in temperature independently of stresses due to the volume change effect (uplift due to ice shell thickening). For the temperature change effect, we were able to obtain numerical results that closely resemble those in Nimmo (2004) when using relatively coarse grids (61 grid points, as used in that work). We found that by increasing the resolution of the mesh, we obtained somewhat higher stresses in the elastic layer of the ice shell. Our results for the volume change effect are very similar to those obtained by Nimmo (2004).

Fourth, we verified that we could reproduce the solutions from Nimmo (2004) while solving the energy equation numerically as opposed to using an analytic solution to the Stefan problem (Stefan, 1891). The results using our numerical solution to the energy equation (including solidification at the ocean/ice interface) converge to those obtained using the analytic solution.

Text S4: Results for thickening ice shells

We calculate the temperature and stresses in a thickening ice shell on Europa and Enceladus in the limit of no internal heating. We assume the initial temperature profile in the ice shell is given by the Stefan solution (Turcotte & Schubert, 2002) and that the ice shell is stress free. Each calculation begins with an initial thickness of 2 km. The models were run for 10 Myr, at which time a thickness of 30 km and cracks no longer reach the ocean on either satellite.

In Figure S2, we show the evolution of tangential stresses, ocean overpressure, and the volume of eruptions for Europa and Enceladus. On Europa, cracks are expected to initiate within the elastic layer (below the surface) and propagate bidirectionally, reaching the surface. No cracks reach the subsurface ocean for the range of ice shell thicknesses considered here. Each failure event is expected to relieve tensile stresses in the ice shell and reduce the ocean overpressure to nearly zero.

On Enceladus, we predict more numerous and more frequent cracking events and we find that it is possible for cracks to reach the ocean. Erupted water volumes (based on the volume required to relieve overpressure) are shown in Figure S2F and are typically close to a global 30 m layer-equivalent, decreasing gradually through time as the ice shell thickens and the amount of overpressure necessary to erupt water increases. Once Enceladus' ice shell becomes thicker than $\sim$ 17 km (Figure S21D), eruptions are no longer possible because the overburden stresses exerted on downward-propagating cracks exceed the tensile stresses. Here, we assume that fractures close and anneal following each eruption event. If fractures remain open (e.g., Kite & Rubin, 2016; Hemingway et al., 2020), we would not

expect the ocean overpressure to increase and we would not expect subsequent fractures to form by the ocean-pressurization mechanism as long as conduits connecting the ocean to the surface remain open.

References

Hemingway, D. J., Rudolph, M. L., & Manga, M. (2020, March). Cascading parallel fractures on Enceladus. *Nature Astronomy*, *4*(3), 234–239. doi: 10.1038/s41550-019-0958-x

Hillier, J., & Squyres, S. W. (1991, August). Thermal stress tectonics on the satellites of Saturn and Uranus. *Journal of Geophysical Research (ISSN 0148-0227)*, *96*, 15665. doi: 10.1029/91JE01401

Kite, E. S., & Rubin, A. M. (2016, April). Sustained eruptions on Enceladus explained by turbulent dissipation in tiger stripes. *Proceedings of the National Academy of Sciences*, *113*(15), 3972–3975. doi: 10.1073/pnas.1520507113

Nimmo, F. (2004). Stresses generated in cooling viscoelastic ice shells: Application to Europa. *Journal of Geophysical Research (Planets)*, *109*, E12001. doi: 10.1029/2004JE002347

Stefan, J. (1891). Über die theorie der eisbildung, insbesondere über die eisbildung im polarmeere. *Ann. Phys*, *278*(2), 269–286.

Timoshenko, S. P., & Goodier, J. N. (1951). Theory of elasticity.

Turcotte, D. L., & Schubert, G. (2002). *Geodynamics* (2nd ed.). New York: Cambridge University Press.

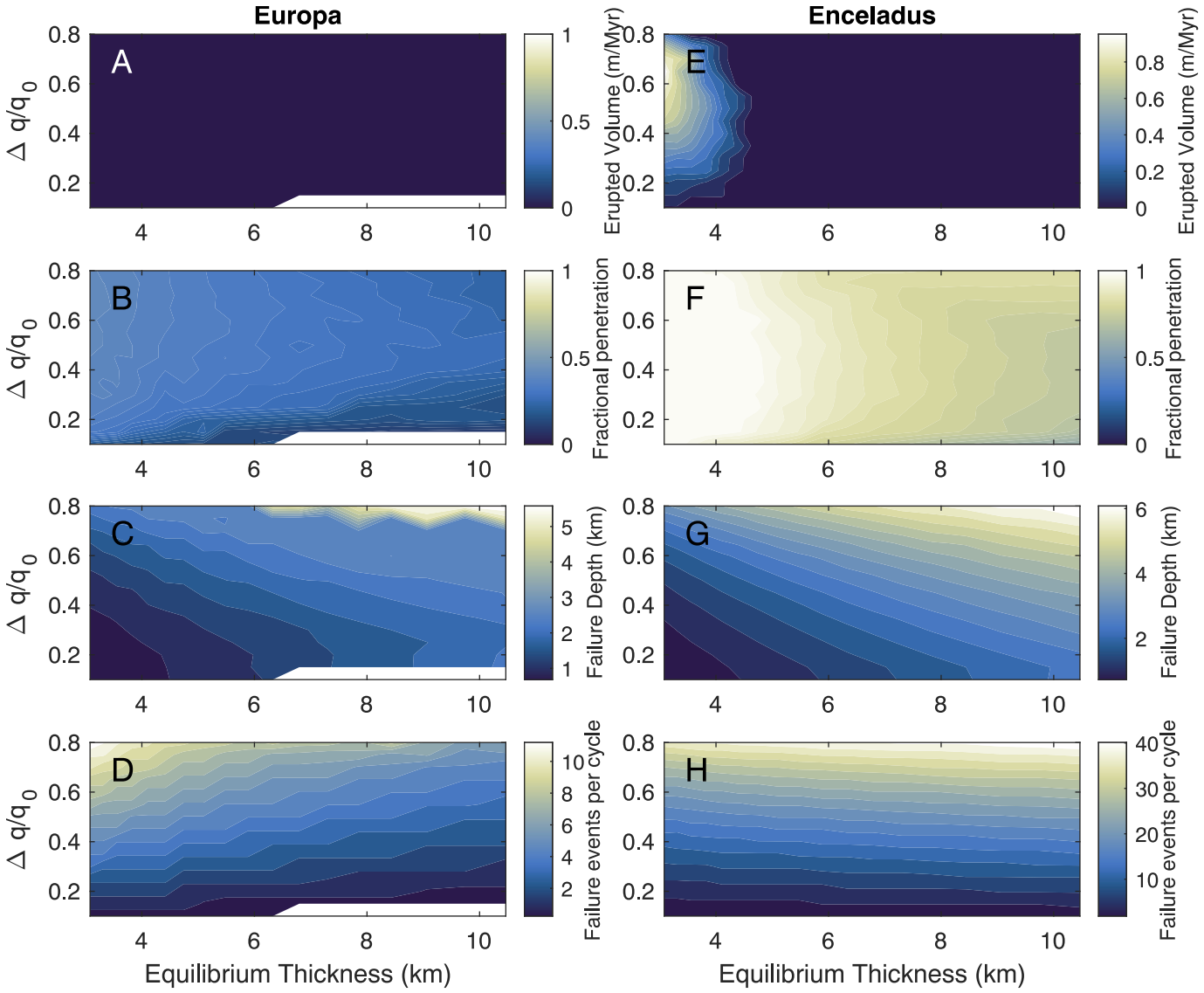

Figure S1. Erupted volume and number of cracking events per 100 Myr oscillatory cycle for Europa (left) and Enceladus (right), assuming a tensile strength of 1 MPa. In (A,D), we show the erupted volume in meters equivalent for each body. (B,E) show fractional penetration of fractures (1.0 corresponds to a fracture that reaches the subsurface ocean). (C.F) show the number of failure events per 100 Myr eccentricity cycle.

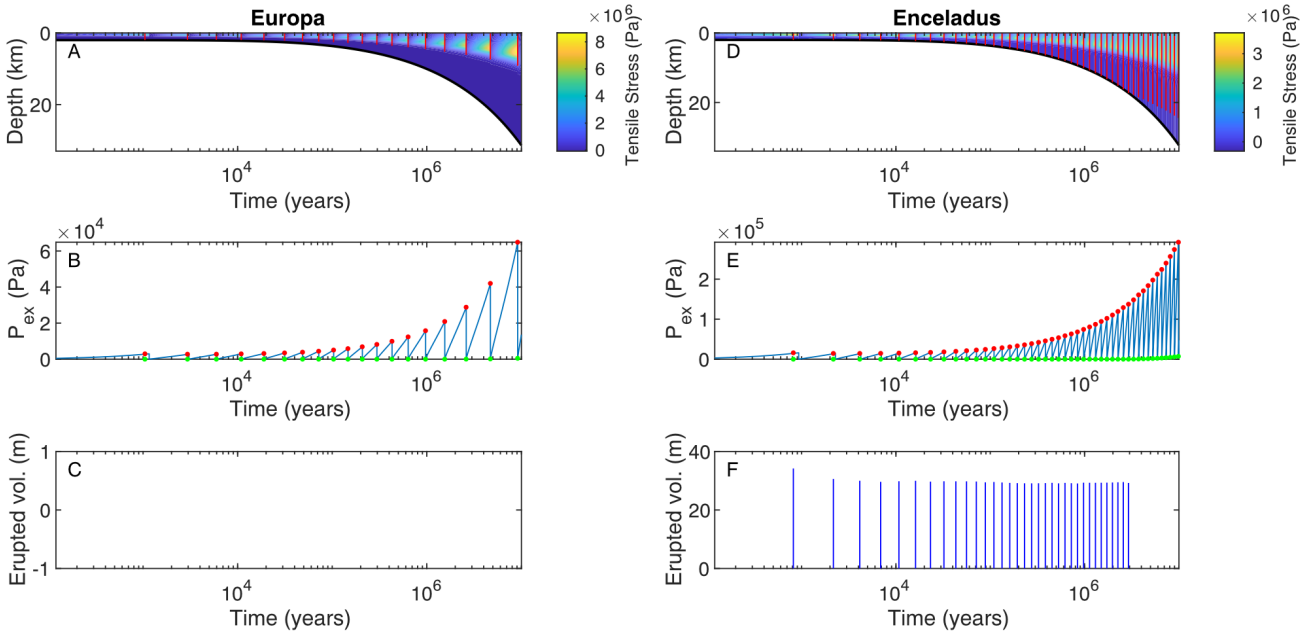

Figure S2. Evolution of tangential stresses σ_t (A,D), ocean overpressure P_{ex} (B,E), and erupted volume (C,F) for Europa (A-C) and Enceladus (D-F). No eruptions are expected on Europa because cracks do not reach the subsurface ocean.

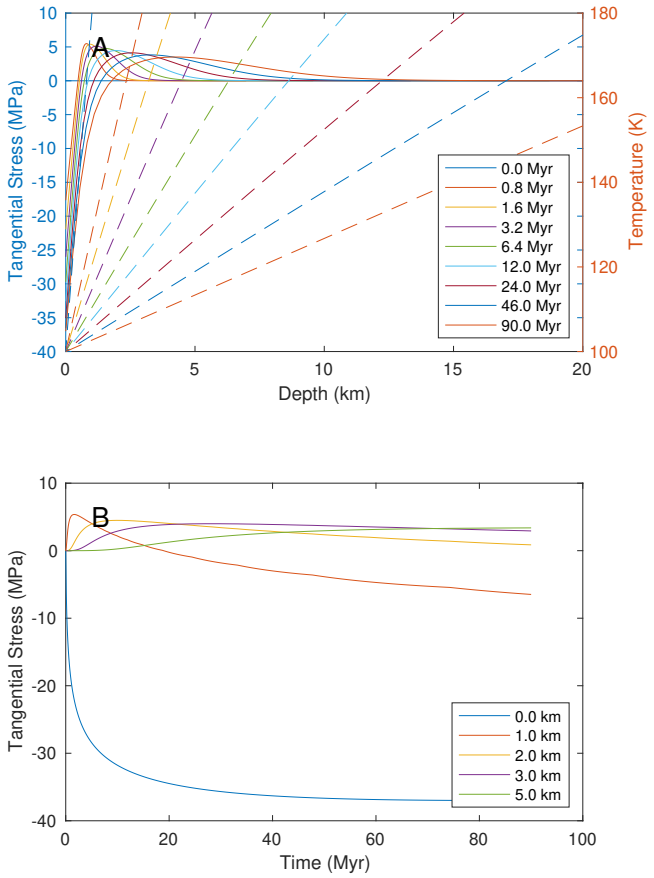

Figure S3. Demonstration of the "temperature change effect" from Nimmo (2004), Figure 1. (a) Tangential stresses (solid lines) at select times given in Myr and temperatures (dashed lines). Tensile stresses are positive. (b) Tangential stresses at selected depths as a function of time.

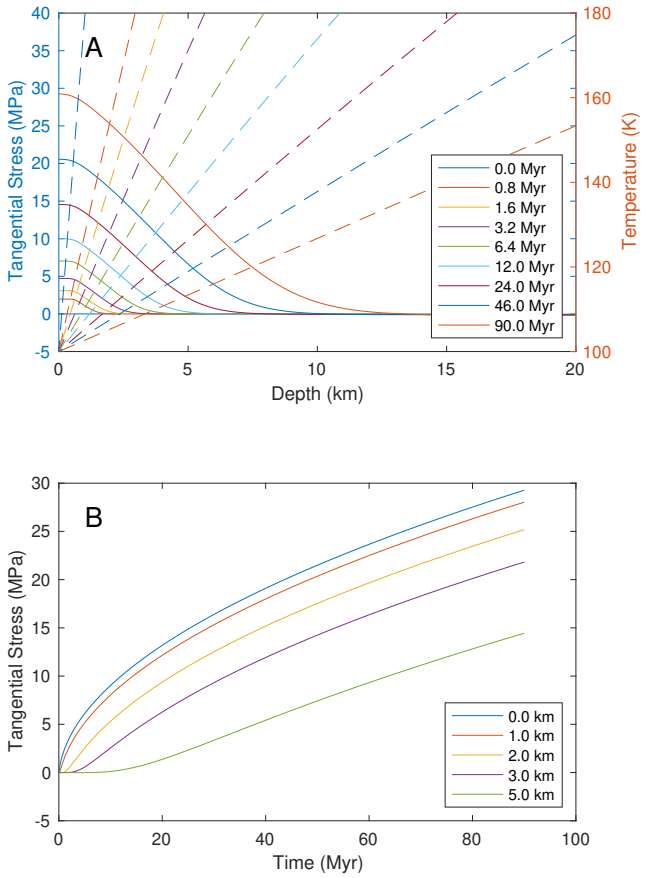

Figure S4. Demonstration of the "volume change effect" from Nimmo (2004), Figure 2. (a) Tangential stresses (solid lines) at select times given in Myr and temperatures (dashed lines). Tensile stresses are positive. (b) Tangential stresses at selected depths as a function of time.

Symbol	Value	Description
ρ_i	917 kg/m^3	ice density
ρ_w	1000 kg/m^3	water density
β_w	4×10^{-10} Pa^{-1}	ocean compressibility
L_f	334 kJ/kg/K	latent heat of fusion
E	5×10^9 Pa	shear modulus
Q	40 kJ/mol	activation energy
μ_b	10^{15} Pa-s	melting-temperature viscosity
T_b	273 K	melting temperature
T_s	100 K	surface temperature

Table S1. Parameters and their values used in our calculations.